THE ASTRONOMICAL JOURNAL, 118:381–389, 1999 July
© 1999. The American Astronomical Society. All rights reserved. Printed in U.S.A.

A MAJOR STAR FORMATION REGION IN THE RECEDING TIP OF THE STELLAR GALACTIC BAR. II. SUPPLEMENTARY INFORMATION AND EVIDENCE THAT THE BAR IS NOT THE SAME STRUCTURE AS THE TRIAXIAL BULGE PREVIOUSLY REPORTED

M. LÓPEZ-CORREDOIRA,[1] F. GARZÓN,[1,2] J. E. BECKMAN,[1,3] T. J. MAHONEY,[1] P. L. HAMMERSLEY,[1] AND X. CALBET[4]
Received 1998 October 12; accepted 1999 March 16

ABSTRACT

This paper is the second part in a series, the first part of which presented an outline of the analysis of 60 spectra from a follow-up program to the Two Micron Galactic Survey (TGMS) project in the $l = 27°$, $b = 0°$ area. In this second part, we present a more detailed explanation of the analysis, a library of the spectra for more complete information for each of the 60 stars, and further discussions on the implications for the structure of the Galaxy. This region contains a prominent excess in the flux distribution and star counts previously observed in several spectral ranges, notably in the TMGS. We found that over 50% of the spectra of the stars detected with $m_K < 5.0$ mag, within a very high confidence level, correspond to stars of luminosity class I, and a significant proportion of the remainder are very late giants that must also be rapidly evolving. We make the case, using all the available evidence, that we are observing a region at the nearer end of the Galactic bar, where the Scutum spiral arm breaks away, and that this is powerful evidence for the presence of the bar. Regions of this type can form because of the concentrations of shocked gas where a galactic bar meets a spiral arm, as is observed at the ends of the bars of many face-on external galaxies. Alternative explanations do not give nearly such a satisfactory account of the observations.

Equivalent spectroscopic analysis should also be performed at $l = -22°$, the candidate position for the other tip of the bar. The space localization of one and a fortiori of both ends of the bar allows us to infer its orientation. If the second region is also confirmed to be a powerful star formation region this would imply a position angle for the bar of about 75° with respect to the Sun–Galactic center line. This geometry is indeed compatible with the range of distances that we have obtained for the star-forming region at $l = 27°$ from spectroscopic parallaxes. However, the angle is different from that given by other authors for the bar, and this, we think, is because they refer to the triaxial bulge and not to the bar as detected here.

Key words: Galaxy: stellar content — Galaxy: structure — stars: formation

1. INTRODUCTION

This paper is the second part of Garzón et al. (1997, hereafter G97) in which we presented an outline of the analysis of 60 spectra from a follow-up program to the Two Micron Galactic Survey (TMGS) project in the $l = 27°$, $b = 0°$ area. This analysis was based on the luminosity classification of stars using the Ca II triplet (Jones, Alloin, & Jones 1984; Díaz, Terlevich, & Terlevich 1989), and a discussion of this region was presented that strengthens the identification of this zone as a star formation region at the receding tip of the stellar bar.

In this second paper, we present the spectra, offer a more detailed explanation of the analysis, and supply more complete information for each of the 60 stars, as well as an extended bibliography and further discussions of the physical morphology.

2. OBSERVATIONS AND DATA REDUCTION

As explained in G97, 70 spectra of stars situated in the region around $l = 27°$, $b = 0°$ selected from the TMGS with $m_K < 5.0$ mag were taken with the Isaac Newton Telescope (INT) at the La Palma Observatory. From these, we had to reject 10 that could not be identified as visible counterparts of TMGS sources. After cross-correlating the original TMGS source positions with their Guide Star Catalogue (Space Telescope Science Institute, 1992) counterparts and then calculating the errors in position, we inferred that TMGS catalog has a positional error box of around 4″ in right ascension by 7″ in declination. The larger error in declination compared with that in right ascension is due to the form of detector array used in the survey (Garzón et al. 1993). This is added to the pointing error of the INT itself and implies that there is a nonnegligible risk of taking the spectrum of the wrong star in such a very crowded area of the sky. By taking spectra of all the bright stars within the error box, we could decide post hoc which candidate was the TMGS object with $m_K < 5.0$ mag from the spectral type and features and I-magnitude estimate. In the 10 cases mentioned above, we could not find any good candidate so these were rejected.

In Table 1 and Figure 1 we give coordinates of all the stars in our sample from the TMGS database. Investigators wishing to use them should be aware that, because of the error of the TMGS coordinates described above and the extremely crowded nature of the field, there is often more than one visible candidate for the infrared source. As we did not use more precise coordinates for a given source, we have not needed to sharpen the precision of these positions.

The extraction of the spectra, sky subtraction, and wavelength calibration were performed using the IRAF tasks

[1] Instituto de Astrofísica de Canarias, E-38200 La Laguna, Tenerife, Spain.
[2] Departamento de Astrofísica, Universidad de La Laguna, E-38204 La Laguna, Tenerife, Spain.
[3] Consejo Superior de Investigaciones Científicas, E-28006 Madrid, Spain.
[4] Instituto Nacional de Meteorología, Santa Cruz, Tenerife, Spain.

TABLE 1

CHARACTERISTICS OF THE STAR SAMPLE

Star No.	R.A.[a]	Decl.[a]	m_K	EW	EW from Eq. No.	Luminosity	Spectral Type	Distance[b] (kpc)
1	18 30 28.2	−5 12 34	3.90	9.2	(2)	I	K5	3.8
2	18 30 52.9	−5 08 24	4.40	8.6	(5)	III	M7	6.9
3	18 31 57.2	−5 13 05	2.50	11.8	(2)	I	K5	2.3
4	18 32 04.3	−5 13 31	4.30	9.3	(5)	I	M3	7.9
5	18 32 17.6	−5 12 34	4.50	11.7	(2)	I	K5	4.7
6	18 32 21.3	−5 14 51	4.10	9.9	(2)	I	K2	4.1
7	18 32 29.0	−5 16 50	4.20	9.8	(2)	I	K5	4.3
8	18 32 33.2	−5 16 49	4.10	8.6	(5)	III	M8	6.3
9	18 32 34.4	−5 14 49	3.80	9.9	(2)	I	F5	1.4
10	18 33 05.3	−5 17 40	4.80	9.6	(2)	I	K5	5.1
11	18 33 06.9	−5 09 47	4.28	8.1	(2)	III	K2	1.2
12	18 34 35.2	−5 11 56	4.74	9.5	(5)	I	M6	8.5
13	18 34 37.3	−5 15 05	3.60	7.7	(5)	III	M5	2.9
14	18 35 12.5,	−5 17 44	3.90	8.0	(2)	III	K0	0.8
15	18 35 35.3	−5 04 01	4.25	9.3	(5)	I	M6	7.9
16	18 35 36.0	−5 03 57	3.70	9.2	(5)	I	M4	6.9
17	18 35 45.4	−5 20 15	4.00	12.7	(2)	I	K5	4.1
18	18 36 23.0	−5 07 04	4.58	10.5	(2)	I	G5	1.9
19	18 37 17.7	−5 16 12	2.20	10.3	(2)	I	K2	2.0
20	18 37 26.0	−5 05 08	4.90	9.3	(5)	I	M8	9.9
21	18 37 45.9	−5 20 29	4.80	9.6	(2)	I	G8	2.1
22	18 37 53.2	−5 04 32	5.00	8.6	(5)	III	M6	7.5
23	18 37 54.5	−5 14 48	3.30	10.8	(2)	I	K2	3.1
24	18 38 05.7	−5 19 37	4.80	10.4	(2)	I	K0	5.2
25	18 38 23.8	−5 15 42	4.52	9.5	(5)	I	M8	8.1
26	18 38 39.2	−5 12 22	4.72	10.6	(2)	I	M0	5.2
27	18 38 50.4	−5 12 31	2.30	11.9	(2)	I	K2	2.1
28	18 39 05.4	−5 12 28	3.70	10.6	(2)	I	K2	3.6
29	18 39 07.1	−5 15 43	4.34	<10.2	(5)	I/III	M8	...
30	18 39 28.2	−5 14 47	4.90	12.4	(2)	I	K5	5.4
31	18 39 32.9	−5 15 19	4.80	8.9	(5)	III	M5	7.5
32	18 39 36.1	−5 16 48	5.00	10.7	(2)	I	K2	5.7
33	18 39 49.8	−5 18 20	2.10	6.0	(2)	III	M2	0.2
34	18 39 58.2	−5 16 45	4.80	9.9	(2)	I	K2	5.2
35	18 40 01.0	−5 14 11	3.60	8.6	(5)	III	M8	5.2
36	18 40 01.7	−5 13 01	5.00	8.6	(2)	III	K0	2.8
37	18 40 38.2	−5 06 45	4.74	<10.2	(5)	I/III	M9	...
38	18 40 49.0	−5 05 23	4.76	6.4	(2)	III	M3	0.9
39	18 40 49.1	−5 05 28	4.60	7.6	(2)	III	G5	0.3
40	18 41 21.2	−5 16 17	4.26	9.5	(2)	I	G2	1.7
41	18 41 55.7	−5 14 16	4.50	10.8	(2)	I	G5	1.8
42	18 42 03.6	−5 04 54	4.36	6.4	(5)	III	M3	0.8
43	18 42 14.3	−5 11 30	4.35	9.9	(5)	I	M7	7.5
44	18 42 17.8	−5 13 06	4.42	9.2	(5)	I	M8	7.5
45	18 42 35.1	−5 16 50	4.42	8.8	(2)	III	K2	2.9
46	18 42 50.2	−5 18 23	4.65	10.7	(2)	I	G2	1.9
47	18 43 15.5	−5 17 48	4.51	9.4	(5)	I	M5	7.7
48	18 43 25.9	−5 11 33	4.40	8.9	(5)	III	M4	6.9
49	18 44 26.2	−5 14 49	4.31	10.3	(2)	I	G5	1.7
50	18 44 47.1	−5 14 51	4.35	9.5	(2)	I	K3	4.6
51	18 45 08.7	−5 12 34	4.45	10.7	(2)	I	G2	1.8
52	18 45 12.4	−5 16 50	4.30	7.9	(2)	III	G5	0.4
53	18 45 34.2	−5 12 33	4.62	6.1	(2)	III	G5	0.1
54	18 45 40.0	−5 07 00	4.46	10.4	(2)	I	G1	1.8
55	18 45 41.9	−5 14 48	4.31	8.5	(2)	III	K3	2.0
56	18 45 43.9	−5 15 21	4.20	9.9	(5)	I	M4	6.9
57	18 45 47.1	−5 17 45	4.69	9.3	(5)	I	M4	9.7
58	18 45 53.6	−5 21 05	4.52	8.3	(2)	III	K7	2.1
59	18 51 37.1	−5 20 11	4.33	7.7	(2)	III	F7	0.3
60	18 54 39.8	−5 11 43	4.39	9.3	(5)	I	M9	8.3

NOTE.—Units of right ascension are hours, minutes, and seconds, and units of declination are degrees, arcminutes, and arcseconds (J2000.0).

[a] Investigators who wish to use the coordinates should be aware that, because of the intrinsic inaccuracies of the TMGS coordinates and the extreme crowding in the field, there is often more than one visible candidate for the IR source.

[b] See G97.

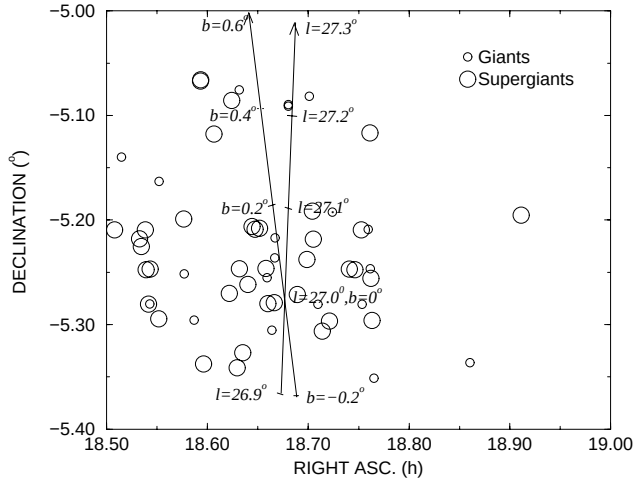

FIG. 1.—Equatorial coordinates (J2000.0) of the stars whose spectra are analyzed in this paper. Small circles stand for giants, and big circles for supergiants.

APEXTRACT and ONEDSPEC, after performing bias subtraction and flat-fielding with CCDRED. The flux was normalized rather than calibrated.

3. LUMINOSITY CLASSIFICATION

Spectra in the zone of the IR Ca II triplet at 8498.02, 8542.09, and 8662.14 Å present in stars of spectral types later than F5 were examined. The triplet was chosen as an optimum differentiator between stars of different luminosity classes. In earlier types, the Paschen hydrogen lines P13 (8665 Å), P15 (8545 Å), and P16 (8502 Å) severely contaminate the spectral region of interest. For spectral types later than M3 or M4, TiO absorption bands mask the Ca II triplet, making its features more difficult to measure, as we will see later.

Measurement of the equivalent width (EW) of the Ca II triplet lines was carried out according to the prescriptions of Díaz et al. (1989) when TiO-band contamination is not present. A continuum $I_\lambda^{\rm cont}$ is defined by a linear fit to the median value of two chosen sidebands centered at 8455 and 8850 Å, respectively, with a width of 15 Å, and the EW was obtained by integrating

$$W_\lambda = \int_{\lambda-15\ \text{Å}}^{\lambda+15\ \text{Å}} \left(1 - \frac{I_{\lambda'}}{I_{\lambda'}^{\rm cont}}\right) d\lambda' \ , \qquad (1)$$

where I_λ is the measured intensity.

We also followed Díaz et al. (1989) in defining

$$\text{EW} = W_{8542\ \text{Å}} + W_{8667\ \text{Å}} \qquad (2)$$

as the indicator of luminosity class. The shortest-wavelength line of the triplet was not used because it is too feeble compared with the neighboring features and yields larger errors in the precise measurement of the total Ca II triplet. Selected reference stars were used to check our EWs, and these were the same within the error margin as those given by Díaz et al. (1989) for the same objects.

The Ca II triplet has been used for many years as an indicator of luminosity class (e.g., Merrill 1934). More recently, Jones et al. (1984) and Díaz et al. (1989) have calibrated empirically the relationship between the EW of the Ca II triplet and the luminosity class for spectral types ranging from F5 to M3. These authors found some dependence of EW on both metallicity and temperature, but these effects were much weaker than the dependence on surface gravity, especially for supergiants. We have followed their results and adopted their criteria in assigning luminosity classes from the measured EWs. From Díaz et al. (1989), if metallicity dependence is assumed negligible, then

$$\log g = 7.75 - 0.65\text{EW} \ . \qquad (3)$$

On this basis, a source is taken to be a supergiant ($\log g$ less than approximately 1.75) if EW > 9 Å, independently of metallicity and temperature. Idiart, Thévenin, & Freitas Pacheco (1997) have demonstrated the presence of correlations of EW with metallicity and temperature, but only for old stars (>1 Gyr) and therefore not for supergiants. There are also other possible luminosity class indicators. In the wavelength range we used, the existence of the CN band (7916–7941 Å) is a characteristic of supergiants (MacConnell, Wing, & Costa 1992), but the Ca II triplet is less affected by noise.

Thirty-eight stars in the sample were not contaminated by the TiO band, and we used the method described above to obtain their EWs in this subsample (see Table 1).

The remaining 22 stars are of later spectral types, and the presence of TiO bands partially masks the triplet lines (see Figs. 6*c* and 6*d*). For these objects we have developed an empirical method that permits the measurement of EW where the Ca II lines are not completely masked by the TiO band. This method uses the depth of the lines instead of the EW.

The depth of the lines is calculated according to

$$\text{depth}_\lambda = 1 - \frac{\min(I_{\lambda'};\ \lambda - 15\ \text{Å} < \lambda' < \lambda + 15\ \text{Å})}{I_\lambda^{\rm cont2}} \ , \qquad (4)$$

where $I_\lambda^{\rm cont2}$ is the value of a new continuum interpolated between two points that are not affected by the TiO absorption: 8432 and 8844 Å.[5]

One potential problem is that the convolution of the profiles of the spectral lines with the instrumental profile would affect the depth of the line, but this effect is in practice negligible compared with the other uncertainties in the method. The convolution with the instrumental profile broadens the line and decreases the depth when the number of pixels defining the line is small. In the lines without TiO contamination, the pixels defining a line cover a sufficient wavelength range for the effect of the convolution to be negligible. In the lines with TiO contamination, the depth is the sum of the TiO band depth and the jump between the TiO band and the peak of the line. If the unblended portion of the line covers a restricted wavelength range, this jump will be affected by the convolution but, as it is small compared with the TiO depth, the effect of the convolution is again small. The effect of convolution would indeed be serious if we were to use Gaussian fits on masked portions of the lines instead of the depth as the measure of equivalent width.

To get the EW as a function of the depth of the deepest line, 8542 Å, it is necessary to use uncontaminated lines. Equation (4) is used for the first 38 stars, those with unmasked Ca II lines, and for these a relationship is then

[5] In fact, a bandwidth of 15 Å between 8417 Å and 8432 Å is selected for which we calculate the median value, and the same is done for the second value of the continuum between 8844 Å and 8859 Å.

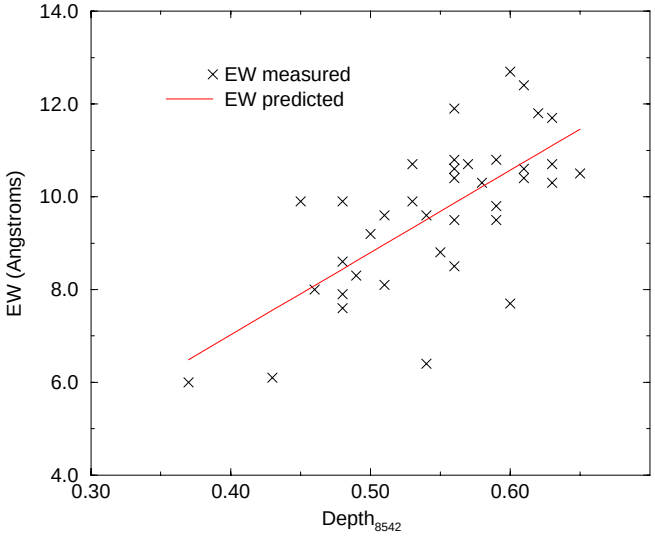

FIG. 2.—Comparison between EW measured in unmasked Ca II lines using eq. (2) and the subsample with the EW obtained via eq. (5).

calibrated between depth_{8542} and the EW calculated using equation (2). The relationship obtained, employing a linear fit, is

$$\text{EW} = -0.1 + 17.8 \times \text{depth}_{8542}\ , \qquad (5)$$

which is plotted together with the data in Figure 2.[6] The use of this expression to evaluate the luminosity class using the criterion of Díaz et al. (1989) is a fair approximation. The fit in equation (5) is a good approximation, but in the latest spectral types other effects may intervene. The EW of the Ca II triplet is not strongly dependent on spectral type, although this dependence is a little more noticeable for M-type stars since the ionization equilibrium in these objects shifts somewhat from Ca II to Ca I (Cohen 1978). One consequence is that this line depth technique may slightly underestimate the number of supergiants. That is, the number of supergiants among stars later than M3 may well be in fact larger than that inferred using the EW > 9 criterion applied to equation (5). Since our purpose is to calculate the fraction of supergiants to determine whether the region studied is a star formation region, this underestimate would change our conclusion only if the answer were negative; but this is not the case, as will be shown below.

Even employing the line depth technique, we had to reject two stars of the sample for which the TiO band gave an unacceptable blend, so we finished with 58 stars with acceptable EWs—38 earlier than M3 and 20 later than M3. The two stars rejected show spectra with no clearly unblended Ca II features; the Ca II + TiO blends show a maximum $\text{depth}_{8542\,\text{Å}}$ from which we may estimate a maximum EW. In both cases, this maximum value of EW is $\approx$10.2 Å, i.e., EW < 10.2, so it could not be decided whether they are giants (EW < 9.0) or supergiants (EW > 9.0). In Table 1, we do show the data for these two stars with EW < 10.2 (stars 29 and 37), but they are not included in either the statistics of the EW or in the distance calculation of paper G97.

The final results of the luminosity classification were shown in Figure 1 of G97, in the form of a histogram of EW frequencies. Those EW values used for the figure are shown in Table 1 for each star.

The ratio of supergiants—those with EW > 9 Å—to the total number of observed objects is most striking. The number of supergiants is in fact 38 out of 58 (66%). In a binomial distribution the root mean square of the distribution is $\sigma = [n \times p \times (1-p)]^{1/2}$, where n is the total number of stars. Here, $n = 58$ stars, $p = 0.66$, so $\sigma = 3.6$ stars. The proportion of supergiants is then $66 \pm 6\%$ ($1\ \sigma$). An error should be added to allow for the possible mistaken classification of giants and supergiants and also to take into account the pointing error of the telescope in a crowded field, which gives a slight chance of taking the spectrum of a wrong star. However, if the "wrong" star turned out to be a late star with sufficient luminosity to give a spectrum of bright star, this would still be indication of late-type giants and supergiants in the zone. These sources of error are small except in the M-type classification, in which the number of supergiants should be even greater than given by our criterion, as discussed above. These considerations lead to the conclusion that the fraction of supergiants is well over 50% with a very high confidence level.

4. SPECTRAL CLASSIFICATION

The spectra of the 60 stars belonging to both subsamples are presented in Figure 6 below, after removing the intrinsic slopes and those due to reddening, in order to show the qualitative differences in the spectra between different kinds of stars. The spectral type classification is carried out for every star by qualitatively comparing the features of our spectra with those of standard stars. The spectral classification is shown in Table 1.

The coolest stars—M3 and later—were compared with those in Bessel (1991), Schulte-Ladbeck (1988), and Barbieri et al. (1981) by inspecting the depth of the TiO band absorption. In Figures 6*c* and 6*d*, it can be seen that there is a growing depression at 8432 and 8844 Å from M3 to M9. Since the features of these sources permit us to differentiate spectral types with an interval of 0.1 or 0.2 spectral types, the classification is quite accurate for these stars.

The earlier type stars were compared with those in Torres-Dodgen & Weaver (1993) and Schulte-Ladbeck (1988), mainly by inspecting lines such as Mg I 8807 Å, Fe I 8612 Å, Fe I–Ti I 8468 Å, O I–Fe I 8446 Å (some of these features are also dependent on luminosity class or metallicity) and Paschen hydrogen lines for those earlier than G2. In this case the errors in the classification could be as large as half a spectral type, except perhaps for those containing Paschen lines.

A histogram of the frequency of spectral types in our sample is shown in Figs. 2 and 3 of G97. As expected, most of the stars are very red and with intrinsic luminosity (see also Calbet et al. 1996a), since TMGS is more sensitive to redder stars. The predominant type among the supergiants is K. Supergiants of very late types are known to exist in very small numbers; we have found a significant number of new examples here. This result is subject to the bias that our method of predicting the EWs gives, where the TiO band affects the Ca II lines; it tends to underestimate the EWs,

[6] The fit to a second-degree polynomial was $\text{EW} = -7.1 + 45.0 \times \text{depth}_{8542} - 25.8 \times \text{depth}^2_{8542}$ which is very close to the linear fit and yields the same values, within the error limits. We emphasize that in G97 we used a second-degree fit, but with a small error, which gave rise to EW values too low by 0.2 or 0.3 Å. This led to our classifying two stars as giants instead of supergiants. This improved result only strengthens our previous conclusions about the proportion of supergiants in the sample.

thereby reducing the apparent fraction of supergiants in the coolest class (M).

5. STELLAR BAR

The conclusion to be drawn from this analysis is that the observed region contains intense star formation of recent origin, since supergiants and bright giants are necessarily young stars. There is a high proportion of young stars, and their high spatial concentration shows that the star formation has taken place in the zone observed. Any associated early B-type or O-type stars, typical of this kind of cluster, are not observed in this case, because their emission in K is too low to reach $m_K < 5$ mag for objects far from the solar neighborhood, and the emission in the visible is very strongly affected by dust extinction.

This star formation region does not belong to the disk or the spiral arms (G97); nor it is likely that it belongs to the ring, as discussed in G97 and Hammersley et al., (1994, hereafter H94). A further convincing reason for excluding a ring, even an elliptical one, besides the ones in those papers, is that it would be prominent in other TMGS regions closer to the center than $l = 27°$ and that the luminosity function of the stellar excess would be invariant, neither of which would be in agreement with the observations. The TMGS star counts after subtraction of a model disk (Wainscoat et al. 1992) and bulge (López-Corredoira et al. 1997) are zero in off-plane directions, showing that those disk and bulge models are good fits to the observations; there is, however, an excess of stars in the plane ($|b| < 2°$). Figure 3 shows a sharp decrease in the star counts in the center, and it also shows that the luminosity function of the stellar excess at $l = 27°$ is different from that in the other regions (the ratio between stars with $m_K \leq 9.0$ mag and $m_K \leq 5.0$ mag is very different). These considerations lead to the conclusion that a ring-type structure, even elongated and eccentric, gives a poor fit to the observations.

A hole in the extinction was suggested as a possible cause of the excess at $l = 27°$ by Jones et al. (1981), but this idea was criticized by Kawara et al. (1982) who observed an invariant $(H-K)$ color for the stars across this region. Also, the TMGS star counts at $l = 27°$ in the plane show an excess of over 100 stars per square degree up to $m_K = 5$, and, according to our calculations, this cannot be satisfactorily explained by assuming that the extinction is zero in that region. Furthermore, CCD VRI photometry of the region shows clearly that the line-of-sight extinction is greater than the standard value of 0.62 mag kpc^{-1} in V (Mahoney 1999; Hammersley et al. 1998).

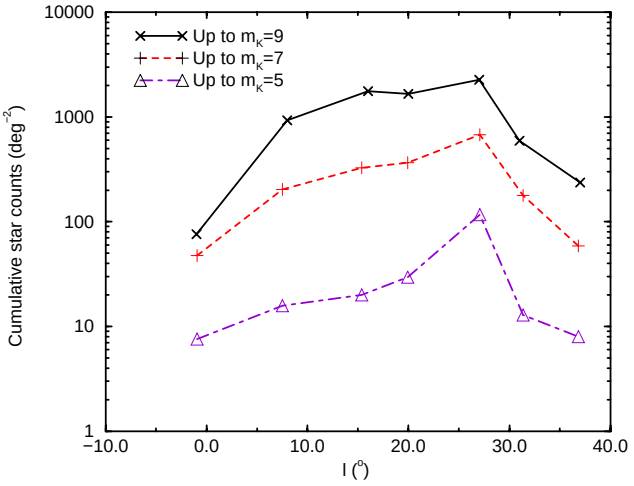

FIG. 3.—TMGS star counts as functions of Galactic longitudes in the Galactic plane after subtraction of the Wainscoat et al. (1992) model disk and the López-Corredoira et al. (1997) model bulge ($b = 0$).

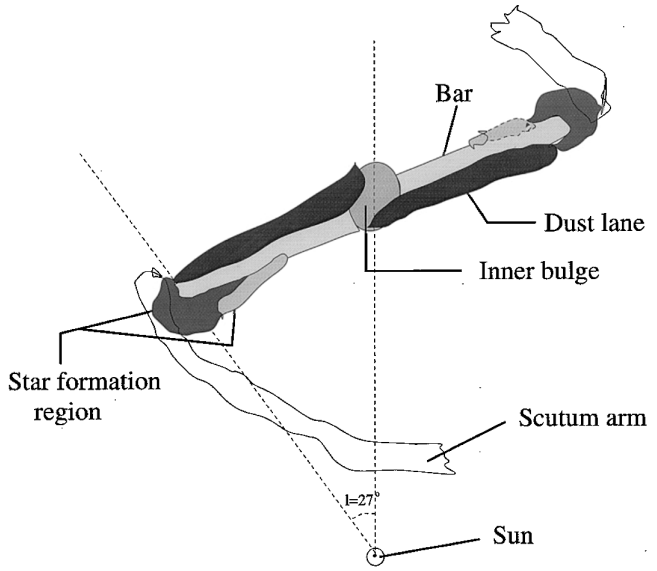

FIG. 4.—Illustration of bar used to explain a number of observations: the excess of extinction at negative Galactic latitudes due to a dust lane (Calbet et al. 1996b) and the star formation regions at each end of the bar.

The most likely explanation is the presence of a giant star formation region which is associated with the receding tip of the stellar Galactic bar (see Fig. 4). If we take the region to be in the center of the star formation region at the end of a bar,[7] it can be used not only as a qualitative demonstration of the bar's existence but also as a means to estimate its orientation. The remaining stars in Figure 3 can be explained as bar stars, with a prominent peak at both ends due to the interaction with spiral arms. Such regions can form because of the concentrations of shocked gas where the Galactic stellar bar meets a spiral arm, as is observed at the ends of the bars of face-on external galaxies (Sandage & Bedke 1994). An excess of extinction at negative latitudes (Calbet et al. 1996b) is also explained by the stellar-bar hypothesis.

This is not the first time that a Galactic bar has been claimed to be discovered, but our arguments in favor of it are new and different from those of other authors. de Vaucouleurs (1964, 1970) first suggested that the Galaxy might be barred in an attempt to explain the observed noncircular gas orbits. Since then, many types of observational evidence have been accumulated that support this hypothesis (see Blitz 1993; Blitz et al. 1993; Kuijken 1996a; Gerhard, Binney, & Zhao 1997). The axial asymmetry of the inner Galaxy is detected by star counts (Nakada et al. 1991; Weinberg 1992; Whitelock, Feast, & Catchpole 1992;

[7] Its center is at $l \sim 27°$, $b \sim 0°$. More precisely, Viallefond et al. (1980) places the region with center at $l = 27°.5$. The region is extended over several degrees but this is the point where the star counts show a maximum which we believe corresponds to the center.

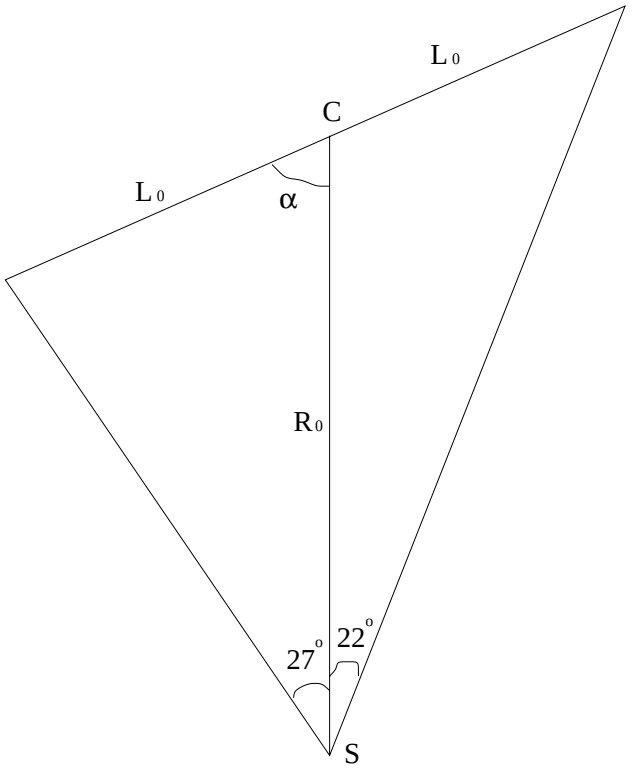

FIG. 5.—Geometry of the bar sustaining an angle α with respect to the Sun ("S")-Galactic center ("C") line.

Stanek et al. 1994, 1996; Wózniak & Stanek 1996; Nikolaev & Weinberg 1997), or by surface photometry at different wavelengths (Blitz & Spergel 1991; Weiland et al. 1994; Dwek et al. 1995; Sevenster 1996), stellar population studies in Baade's window (Ng et al. 1996), microlensing (Paczyński et al. 1994) and studies of the extinction using lensed stars (Stanek 1995), analysis of internal motions of the gas (Peters 1975; Liszt & Burton 1980; Yuan 1984; Gerhard 1996). Models including a bar (e.g., Binney et al. 1991; Zhao 1996) can explain these observational features.

Not all of these observations necessarily imply the existence of a bar; some could be explained by a triaxial structure in the inner Galaxy. Whether this structure is a triaxial bulge, or whether a bar or both features are present is still a matter of controversy (Kuijken 1996b; Ng 1998), and there are reasons for believing that many authors who refer to a bar are in fact referring to the triaxial bulge.

In our previous analysis of the TMGS database (Garzón et al. 1993) we described evidence in favor of the presence of a triaxial bulge (López-Corredoira et al. 1997) with radial scale length of approximately 2.2 kpc, making an angle 12° with respect to the Sun-Galactic center line in the first quadrant, in strong agreement with the angle given by many other authors (Binney et al. 1991; Weinberg 1992; Dwek et al. 1995; Binney, Gerhard, & Spergel 1997; Stanek et al. 1997; Nikolaev & Weinberg 1997) whose bar angle (around 20°) is quite close to this. The bar of this paper must be a different structure from the triaxial bulge, because the inclination of the bulge is not sufficient for a bar tip to reach $l = 27°$ or for a dust lane to reach $l = -19°$ at the other side of the bar, as found by Calbet et al. (1996b). The triaxial bulge reported by López-Corredoira et al. (1997) does not yield sufficient star counts in the plane at positive Galactic latitudes, taking into account the disk and the extinction, to explain the observations.

There is another infrared peak at negative Galactic longitudes at $l = -22°$, which is very similar to the one analyzed here.[8] If we assume that the other end of the bar is at $l = -22°$, the orientation of the bar can be derived. In fact, it is a simple trigonometrical problem if we take the bar to be rectilinear and of equal length from each end to the center.

Applying the sine rule (see Fig. 5),

$$\frac{L_0}{\sin 27°} = \frac{R_0}{\sin (180° - 27° - \alpha)}, \tag{6}$$

$$\frac{L_0}{\sin 22°} = \frac{R_0}{\sin (\alpha - 22°)}. \tag{7}$$

Hence, with $R_0 = 7.86$ kpc (López-Corredoira et al. 1997), we deduce that $\alpha = 75.^{\circ}6$ and the length of the bar from tip to tip is $2L_0 = 7.4$ kpc.

Therefore, we suspect that authors who give a much lower angle are in fact analyzing the angle of the triaxial bulge or an average angle of the composition of both bulge and bar, instead the bar angle. The triaxial bulge cannot be causing the features seen at $l = 27°$.

We can also derive geometrically the distance to the tip at $l = 27°$ as being 7.8 kpc. This distance is compatible with that derived in G97 (in Table 1 are the distances for each star), taking into account all the uncertainties in the calculation.

6. CONCLUSIONS

This paper, together with its first part (G97) makes a spectroscopic analysis of the brightest stars in an infrared-selected sample of objects close (Fig. 6) to the Galactic plane at $l = 27°$, showing a strikingly high fraction of supergiants, which is characteristic of a strong star formation region.

We argue, using all the available evidence, that this region is situated at one end of the Galactic bar, where the Scutum spiral arm breaks away, and that the presence of the region is itself a powerful evidence for the presence of the bar. None of the alternative possibilities (arm, disk, bulge, or ring components) is capable of explaining the observations in a satisfactory manner.

The detected presence of a similar concentration of near-IR sources in the plane at $l = -22°$ should, on this hypothesis, indicate the other end of the bar. To confirm this requires a similar spectroscopic campaign to that reported here. A rectilinear bar between these two points makes an angle of 75° with the Sun–Galactic center line and has a total length of 7.4 kpc. The distance this implies to the star-forming zone analyzed here is consistent with the estimated spectroscopic parallaxes of the stars whose spectra we have analyzed in the first part of the paper (G97), giving a self-consistent picture of the bar.

It is important to distinguish this bar from the triaxial bulge of the Galaxy (López-Corredoira et al. 1997). Many of the previous claims to describe a Galactic bar are more likely to refer to the triaxial bulge and not to the bar.

[8] See *COBE*-DIRBE data (Boggess et al. 1992) or near-infrared catalogs which cover the Galactic plane at positive and negative Galactic longitudes. See also H94 and Calbet et al. (1996b).

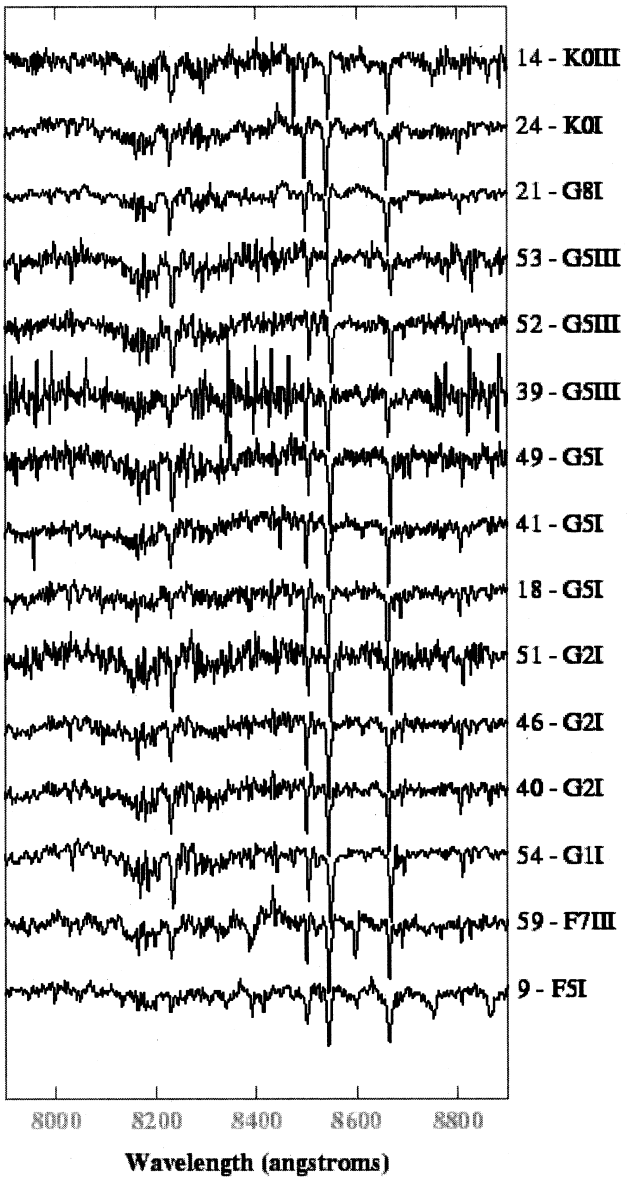

FIG. 6*a*

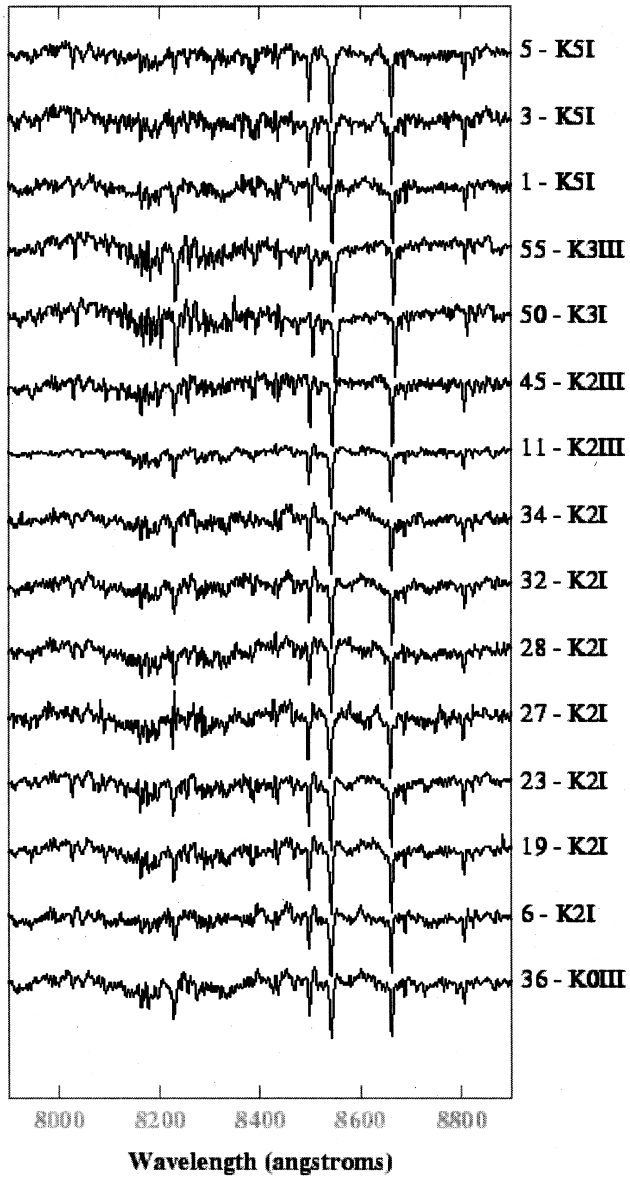

FIG. 6*b*

FIG. 6.—Plots of the spectra from our sample in the range 7900–8900 Å. The intrinsic slopes and those due to reddening have been removed. Numbers for the stars in the right-hand side correspond to those given in the first column of Table 1 and to the spectral type (seventh col.) and luminosity class (eighth col.) of the star.

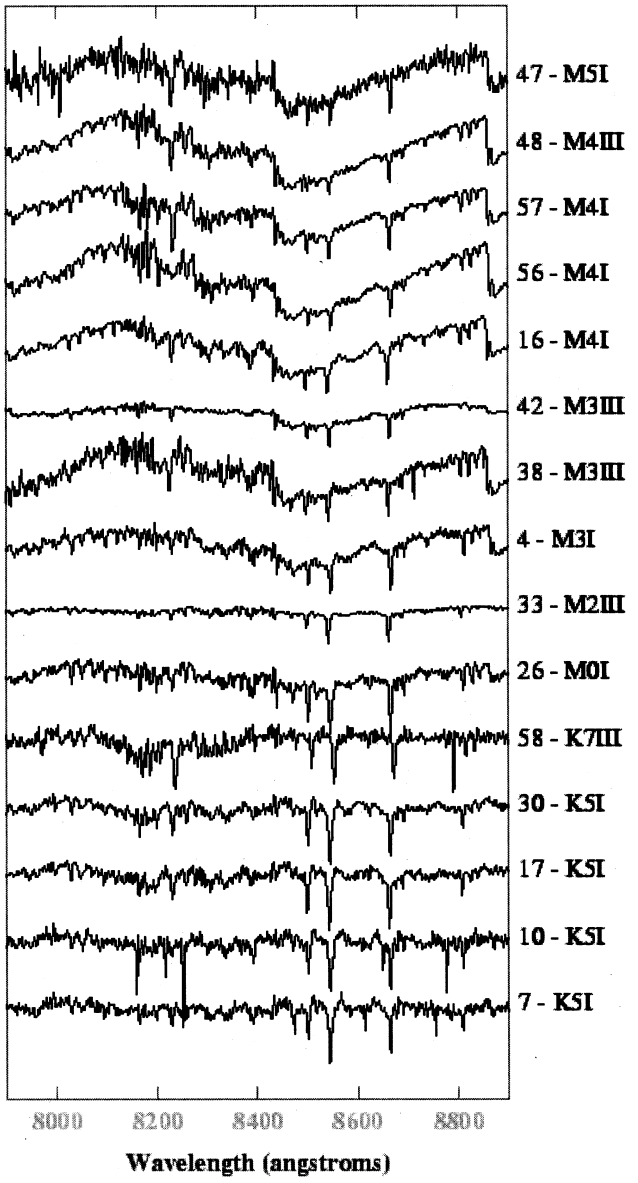
47 - M5I
48 - M4III
57 - M4I
56 - M4I
16 - M4I
42 - M3III
38 - M3III
4 - M3I
33 - M2III
26 - M0I
58 - K7III
30 - K5I
17 - K5I
10 - K5I
7 - K5I
8000
8200
8400
8600
8800
Wavelength (angstroms)

FIG. 6*c*

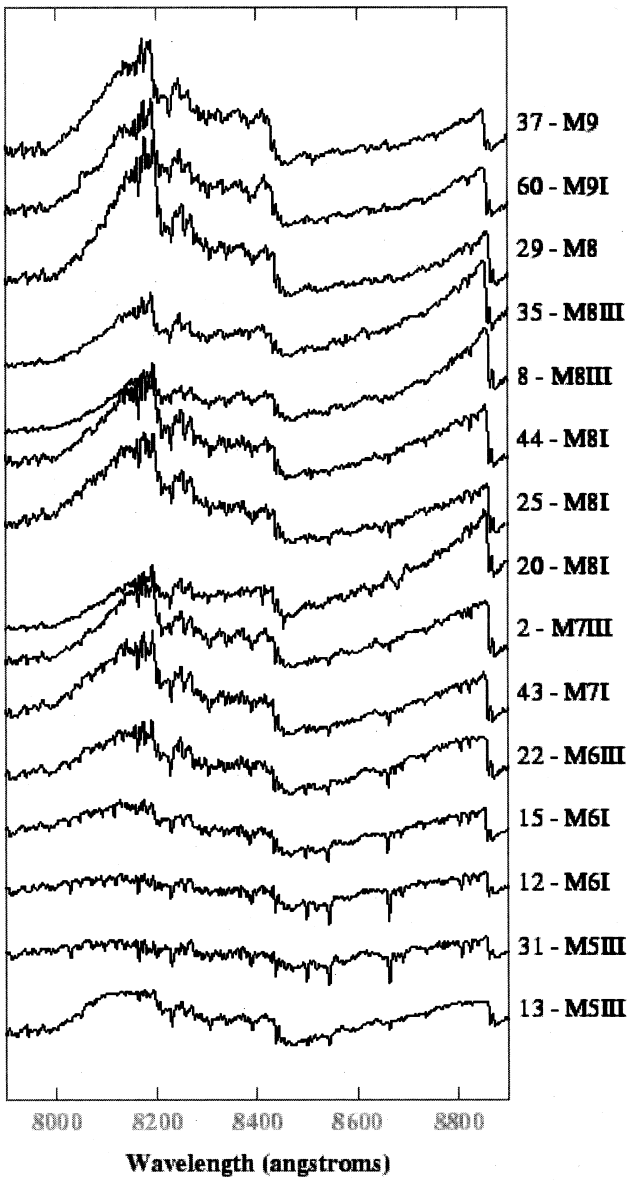
37 - M9
60 - M9I
29 - M8
35 - M8III
8 - M8III
44 - M8I
25 - M8I
20 - M8I
2 - M7III
43 - M7I
22 - M6III
15 - M6I
12 - M6I
31 - M5III
13 - M5III
8000
8200
8400
8600
8800
Wavelength (angstroms)

FIG. 6*d*

The Isaac Newton Telescope is operated on the island of La Palma by the Royal Greenwich Observatory in the Spanish Observatorio del Roque de Los Muchachos of the Instituto de Astrofísica de Canarias. This work was partially supported by grants PB94-1107 and PB97-0219 of the Spanish DGICYT.

REFERENCES

Barbieri, C., Bonoli, C., Bortoletto, F., di Serego, S., & Falomo, R. 1981, Mem. Soc. Astron. Italiana, 52, 195
Bessel, M. S. 1991, AJ, 101, 662
Binney, J., Gerhard, O. E., & Spergel, D. 1997, MNRAS, 288, 365
Binney, J., Gerhard, O. E., Stark, A. A., Bally, J., & Uchida, K. I. 1991, MNRAS, 252, 210
Blitz, L. 1993, in AIP Conf. Proc. 278, Back to the Galaxy, ed. S. S. Holt & F. Verter (New York: AIP), 98
Blitz, L., Binney, J., Lo, K. Y., Bally, J., & Ho, P. T. P. 1993, Nature, 361, 417
Blitz, L., & Spergel, D. N. 1991, ApJ, 370, 205
Boggess, N. W., et al. 1992, ApJ, 397, 420
Calbet, X., et al. 1996a, in New Extragalactic Perspectives in the New South Africa, ed. D. L. Block, & J. Mayo Greenberg (Dordrecht: Kluwer), 532
Calbet, X., Mahoney, T., Hammersley, P. L., Garzón, F., & López-Corredoira, M. 1996b, ApJ, 457, L27
Cohen, J. G. 1978, ApJ, 221, 788
de Vaucouleurs, G. 1964, in IAU Symp. 20, The Galaxy and the Magellanic Clouds, ed. F. J. Kerr & A. W. Rodgers (Canberra: Australian Acad. Sci.), 195
———. 1970, in IAU Symp. 38, The Spiral Structure of Our Galaxy, ed. W. Becker & G. Contopoulos (Dordrecht: Reidel), 18
Díaz, A. I., Terlevich, E., & Terlevich, R. 1989, MNRAS, 239, 325
Dwek, E., et al. 1995, ApJ, 445, 716
Garzón, F., Hammersley, P. L., Mahoney, T., Calbet, X., Selby, M. J., & Hepburn, I. D. 1993, MNRAS, 264, 773
Garzón F., López-Corredoira, M., Hammersely, P., Mahoney, T. J., Calbet, X., & Beckman, J. E. 1997, ApJ, 491, L31 (G97)
Gerhard, O. E. 1996, in IAU Symp. 196, Unsolved Problems of the Milky Way, ed. L. Blitz & P. Teuben (Dordrecht: Kluwer), 79
Gerhard, O. E., Binney, J., & Zhao, H. 1997, Highlights Astron. 11, ed. J. Andersen (Dordrecht: Kluwer)
Hammersley, P. L., Garzón, F., Mahoney, T., & Calbet, X. 1994, MNRAS, 269, 753 (H94)
Hammersley, P. L., Garzón, F., Mahoney, T., & López-Corredoira, M. 1998, in The Impact of Near-infrared Sky Surveys on Galactic and Extragalactic Astronomy, ed. N. Epchtein (Dordrecht: Kluwer), 63
Idiart, T. P., Thévenin, F., & de Freitas Pacheco, J. A. 1997, AJ, 113, 1066
Jones, J. E., Alloin, D. M., & Jones, B. J. T. 1984, ApJ, 283, 457
Jones, T. J., Ashley, M., Hyland, A. R., & Ruelas-Mayorga, A. 1981, MNRAS, 197, 413
Kawara, K., Kozasa, T., Sato, S., Kobayashi, Y., Okuda, H., & Jugaku, J. 1982, PASJ, 34, 389
Kuijken K. 1996a, in IAU Colloq. 157, Barred Galaxies, ed., R. Buta, B. G. Elmegreen, & D. A. Crocker (San Francisco: ASP), 504
Kuijken K. 1996b, in IAU Symp. 196, Unsolved Problems of the Milky Way, ed. L. Blitz & P. Teuben (Dordrecht: Kluwer), 71
Liszt, H. S., & Burton, W. B. 1980, ApJ, 236, 779
López-Corredoira, M., Garzón, F., Hammersley, P. L., Mahoney, T. J., & Calbet, X. 1997, MNRAS, 292, L15
MacConnell, D. J., Wing, R. F., & Costa, E. 1992, AJ, 104, 821
Mahoney, T. J. 1999, in preparation
Merrill, P. W. 1934, ApJ, 79, 183
Nakada, Y., Onaka, T., Yamamura, I., Deguchi, S., Hashimoto, O., Izumiura, H., & Sekiguchi, K. 1991, Nature, 353, 140
Ng, Y. K. 1998, in IAU Symp. 184, The Central Regions of the Galaxy and Galaxies, ed. Y. Sofue (Dordrecht: Kluwer), 27
Ng, Y. K., Bertelli, G., Chiosi, C., & Bressan A. 1996, A&A, 310, 771
Nikolaev, S., & Weinberg, M. D. 1997, ApJ, 487, 885
Paczyński, B., Stanek, K. Z., Udalski, A., Szymański, M., Kałużny, J., Kubiak, M., Mateo, M., & Krzemiński, W. 1994, ApJ, 435, L113
Peters, W. L. 1975, ApJ, 195, 617
Sandage, A., & Bedke J. 1994, The Carnegie Atlas of Galaxies (Washington: Carnegie)
Schulte-Ladbeck, R. E. 1988, A&A, 189, 97
Sevenster, M. N. 1996, in IAU Colloq. 157, Barred Galaxies, ed., R. Buta, B. G. Elmegreen, & D. A. Crocker (San Francisco: ASP), 536
Space Telescope Science Institute. 1992, The Guide Star Catalog, version 1.1 (Baltimore: STScI)
Stanek, K. Z. 1995, ApJ, 441, L29
Stanek, K. Z., Mateo, M., Udalski, A., Szymański, M., Kałżuny, J., & Kubiak, M. 1994, ApJ, 429, L73
Stanek, K. Z., et al. 1996, in IAU Colloq. 157, Barred Galaxies, ed., R. Buta, B. G. Elmegreen, & D. A. Crocker (San Francisco: ASP), 545
Stanek, K. Z., Udalski, A., Szymański, M., Kałużny, J., Kubiak, M., Mateo, M., & Krzemiński, W. 1997, ApJ, 477, 163
Torres-Dodgen, A. V., & Weaver, W. M. B. 1993, PASP, 105, 693
Viallefond, F., Léna, P., de Muizon, M., Nicollier, C., Rouan, D., & Wijnbergen, J. J. 1980, A&A, 83, 22
Wainscoat, R. J., Cohen, M., Volk, K., Walker, H. J., & Schwartz, D. E. 1992, ApJS, 83, 111
Weiland, J. L., et al. 1994, ApJ, 425, L81
Weinberg, M. D. 1992, ApJ, 384, 81
Whitelock, P. A., Feast, M. W., & Catchpole, R. M. 1991, MNRAS, 248, 276
Woźniak, P. R., & Stanek, K. Z. 1996, ApJ, 464, 233
Yuan, C. 1984, ApJ, 281, 600
Zhao H. 1996, in IAU Colloq. 157, Barred Galaxies, ed. R. Buta, B. G. Elmegreen, & D. A. Crocker (San Francisco: ASP), 549